Title

Large scale 3D EM inversion using optimized simulation grids nonconformal to the model space

Authors

Commer, M

Newman, GA

Publication Date

2018

Peer reviewed

Large scale 3D EM inversion using optimized simulation grids nonconformal to the model space

Michael Commer and Gregory A. Newman, Lawrence Berkeley National Laboratory, Berkeley, California

SUMMARY

We analyse a strategy to optimize the computational effort of large-scale electromagnetic (EM) modeling and particularly inversion, the latter usually requiring a large number of forward modeling solutions. While we are interested in finely gridded earth models to capture realistic structures, the forward modeling operator may act upon a coarser simulation grid, or a subsection of the model grid, thus providing significant potential for computational speed-up. After briefly outlining the methodology of the grid transfers and its implications on the inversion scheme, we demonstrate the method on a marine CSEM survey example.

INTRODUCTION

Three-dimensional (3D) conductivity imaging of EM data has become increasingly important, owing to new exploration scenarios, as for example the marine environment, and new efforts of combining the capabilities of EM with those of more "traditional" seismic based methods. Realistic parameterizations of the earth's conductivity may involve a large and fine mesh, leading to as many as $10^6 - 10^7$ grid cells, in order to correctly simulate highly structured 3D geology, bathymetry, or topography. However, depending on the excitation frequency, be it either from a natural or a controlled source, the characteristics of the EM field to be simulated may allow for a discretization with a lower degree of spatial sampling. Key to using this advantage is an appropriate mapping scheme to transfer between the vector based quantities on the simulation mesh and the scalar-type conductivity parameters on the modeling mesh.

METHOD

We consider a modeling/inversion grid Ω_m of size (number of cells) M and a finite-difference (FD) simulation grid Ω_s of size N. Both grids are Cartesian with conformal grid axes, with Ω_s based on a staggered Yee (1966) grid. Ω_m defines the space of the model parameters, i.e. electrical conductivities $\sigma_k,\ k = 1,\ldots,M$, that are assigned to cell centers. The inversion domain will be either Ω_m or a subset. In the inverse problem, we want to determine the distribution of σ over the inversion grid such that a set of observed measurements is reproduced. Solving the inverse problem is in principal accomplished by the iterative minimization of a cost functional Φ, denoting the misfit between observed and predicted data (e.g. Newman & Alumbaugh, 1997). This requires computing the gradient $\nabla\Phi$ with respect to the model parameters σ_k, with its components $\frac{\partial\Phi}{\partial\sigma_k}$.

A full derivation of the gradient formulation for the 3D EM inverse problem, using a scattered-field formulation, is given by Newman & Alumbaugh (1997) and Newman & Hoversten (2000). Here, we only outline the differing methodology resulting from the case $\Omega_m \neq \Omega_s$. The first linking point between the simulation grid and the grid defining the model parameter space occurs in the construction of the $3N \times 3N$ FD stiffness matrix $\mathbf{K}$ of the linear system

$$\mathbf{KE} = \mathbf{S}, \tag{1}$$

which denotes the forward modeling problem. See for example Alumbaugh et al. (1996) for details. In equation (1), $\mathbf{S}$ is the source vector that depends on the boundary conditions, source field polarization, and excitation frequency, and $\mathbf{E}$ is the electric field solution vector. Both vectors belong to the edge element space defined by Ω_s. Construction of $\mathbf{K}$ further requires the vector

$$\Sigma = \{\sigma_1^x, \sigma_1^y, \sigma_1^z, \ldots, \sigma_l^x, \sigma_l^y, \sigma_l^z, \ldots, \sigma_N^x, \sigma_N^y, \sigma_N^z\} = \{\sigma_1^e, \ldots, \sigma_n^e, \ldots, \sigma_{3N}^e\}$$

of edge-based directional conductivities. In the case $\Omega_m = \Omega_s$, an element of Σ is computed from

$$\sigma_n^e = \sum_{i=1}^{4} \sigma_i^n w_i^n, \qquad w_i^n = \frac{dV_i^n}{\sum_{j=1}^{4} dV_j^n}, \tag{2}$$

where w_i are weights determined by volume fractions. In this case, the function mapping from Ω_m to Ω_s is a weighted average of the four model cell conductivities σ_i^n connected by the edge n. From a reversed point of view, a cell conductivity σ_k contributes to the averages of 12 edge conductivities. Note, that this only holds for inner grid cells with no face being part of the grid boundary $\partial\Omega_s$.

Computation of the gradient vector $\nabla\Phi$ also requires mapping between the different grids, this time from Ω_s to Ω_m, because the gradient contains the data sensitivities (Newman & Hoversten, 2000)

$$\frac{\partial \mathbf{E}}{\partial \sigma_k} = \mathbf{K}^{-1}\left(\frac{\partial \mathbf{S}}{\partial \sigma_k} - \frac{\partial \mathbf{K}}{\partial \sigma_k}\mathbf{E}\right), \tag{3}$$

as can be derived from equation (1). Since with every electric field component, one has one equation in the system (1), it follows that the derivatives $\frac{\partial \mathbf{S}}{\partial \sigma_k}$ and $\frac{\partial \mathbf{K}}{\partial \sigma_k}$ each have 12 non-zero entries.

In the case $\Omega_s \neq \Omega_m$, we employ a material averaging scheme based on an integro-interpolation method (Moskow et al. 1999). This allows for an arbitrary translation, assuming conformal grid axes, between Ω_s and Ω_m. Exemplified for the x-edge at grid node (i, j) in a 2D case, one has

$$\sigma_{(i,j)}^x \left[\int_{hi}^{h(i+1)} \left(\int_{h(j-1/2)}^{h(j+1/2)} \sigma(X)dy\right)^{-1} dx\right]^{-1}. \tag{4}$$

Here, a uniform grid $\Omega_s = x^{ij} = (hi, hj)$ is assumed. The inner integral of (4) produces the effective conductivity owing to a parallel circuit representation of conductors $\sigma(X)$. The outer integration represents a serial circuit of all resistors along the total edge length $\int_x dx$. In 3D one has in a discrete formulation

$$\sigma_n^e = \left[\sum_{j=1}^{J(n)} \left(\frac{1}{V_j}\sum_{i=1}^{I_j} dV_i\sigma_i\right)^{-1} \Delta x_j\right]^{-1} \Delta X(n), \tag{5}$$

where

- $\Delta X(n)$=length of the edge n, equals the size of the corresponding simulation grid cell l along the edge's Cartesian orientation.
- $J(n)$=number of discrete parallel circuits P_j along $\Delta X(n)$,
- V_j=total volume of a discrete parallel circuit P_j,
- I_j=number of cells included in the volume V_j or overlapped by V_j,
- dV_i=volume fraction of σ_i contributing to a parallel circuit P_j,

- Δx_j=segment length of the parallel circuit P_j; note that $\sum_{j=1}^{J(n)} \Delta x_j = \Delta X(n)$.

Note that, in contrast to (2), we now omit the superscript n for σ_i and dV_i. When computing an x, y, or z-oriented edge conductivity, the integration direction of (5) corresponds to this Cartesian orientation.

Reviewing equation (3), the data sensitivity for the kth model parameter has non-zero entries for these edges n that have a contribution from σ_k through the corresponding average (5). If we denote the number of edge contributions by $N_e(k)$, applying the chain rule gives for example

$$\frac{\partial \mathbf{K}}{\partial \sigma_k} = \sum_{n=1}^{N_e(k)} \frac{\partial \mathbf{K}}{\partial \sigma_n^e} \frac{\partial \sigma_n^e}{\partial \sigma_k}, \tag{6}$$

and a similar expression for $\frac{\partial \mathbf{S}}{\partial \sigma_k}$. The inner derivatives $\frac{\partial \sigma_n^e}{\partial \sigma_k}$ of (6) are obtained by again applying the chain rule to (5),

$$\frac{\partial \sigma_n^e}{\partial \sigma_k} = \frac{\sigma_n^{e\,2}}{\Delta X(n)} \sum_{j=1}^{J(k)} \Delta x_j \left(\frac{1}{V_j} \sum_{i=1}^{I_j} dV_i \sigma_i \right)^{-2} \frac{dV_k}{V_j}.$$

Here, we denote as $J(k)$ the number of segments, or parallel circuits P_j, with a non-zero contribution from σ_k. For $\Omega_s = \Omega_m$, one has $J(k) = 1$, $\Delta x_1 = \Delta X(n)$, and hence $\frac{\partial \sigma_n^e}{\partial \sigma_k} = \frac{dV_k}{V_1} = w_k^n$, which is the corresponding weighting coefficient of the average (2).

MARINE CSEM SURVEY EXAMPLE

We present an inversion example using synthetic data simulated in a marine environment. Figure 1 shows the true model, the inversion result, and the simulated transmitter-receiver profiles (Figure 1, upper left). Three profiles run accross a resistive target (50 $\Omega \cdot$m), embedded into a 0.7 $\Omega \cdot$ m background. Each profile has 7 horizontal electric dipole sources of length 200 m, oriented parallel to the profile, located 50 m above the seafloor, and with spacing intervals Δ =1000 m for profiles 1 and 2, and Δ =1400 m for profile 3. The receivers, located on the seafloor at z =0 m, are separated by a distance Δ =100 m (p. 1, 2) and Δ =140 m (p. 3). Inline electric fields are sampled on profiles 1 and 2, and both E_x and E_y are sampled on profile 3.

Each source operates at the three frequencies 0.25 Hz, 0.75 Hz, and 1.25 Hz. Hence, computation of the predicted data at each inversion iteration effectively requires 63 forward solutions, with a total sum of 19362 data points. For each frequency we employed a different simulation grid, with the uniform grid node spacing adapted to the frequency, i.e. 75 m for 1.25 Hz, 100 m for 0.75 Hz, and 125 m for 0.25 Hz. For a comparison, we also carried out an inversion using one mesh, the finest (75 m spacing) of the three simulation meshes, for all sources. To enforce some independence of the synthetic data from the employed simulation grids, we created the data using an even finer node spacing of 50 m. Furthermore, three percent noise with a Gaussian distribution was added to the data. The inversion domain covers 90 %, without the water layer, of the model space, starting right below the seafloor. The model grid of size $134 \times 134 \times 134$ has a uniform spacing of 75 m and thus conforms to the simulation grid used for the 1.25 Hz signals. The inversion domain extends over most of the model domain below the seafloor and includes over 1047816 cells.

The (top and bottom) pairs of Figure 1 compare the resulting model after 200 iterations, showing horizontal sections (a,b) and a vertical section through $y = 0$ m (c). While the horizontal extensions of the resistor are fairly well reproduced, both results suffer from an inferior vertical resolution of the target location. We have experienced that by allowing more iterations, this can be mitigated. Furthermore, a broader frequency band is likely to increase the vertical resolution. In general, both inversions clearly indicate the resistive target. For the three-mesh inversion, one can observe a slightly less pronounced resistor at 1200 m depth, compared to the single-mesh result (Figure 1b). This also reflects in a comparison of the total data misfits, shown in Figure 2. While the initial misfit is similar for both inversions, the error produced by the three-mesh inversion drops at a slightly slower rate after 10 iterations, however continues with a generally similar rate of decrease. A comparison of the data fits between the inverted data, also referred to as observed data, and predicted data is given for profile 1 and the frequency 0.25 Hz in Figures 3(a)-3(c), where (a) depicts the initial fit. Comparing the final fits in Figures 3(b) and 3(c), one observes only small differences at large offsets between both inversions.

Table 1: Computational requirements for the inverse solutions using a single (fine) mesh and three different meshes.

	single mesh	3 meshes
Total computation time (Hours):	27.1	15.3
Average computation time per inversion iteration (Seconds):	484	273

It can be concluded that the larger misfit of the three-mesh result is probably caused by some loss of accuracy when using simulation grids with a spatial sampling rate that is coarser than the actual model parameterization. However, the similar inversion results show that this carries over to the resolution of the parameter space to only a minor degree.

We used 448 processors of a distributed memory computer (IBM p575 POWER 5) of the NERSC* computing facilities to carry out the inversions. The computation times are summarized in Table 1.

CONCLUSIONS

We have made significant progress in developing a new method for further reducing the computationally high demands of the large-scale EM inverse problem. Being able to separate the simulation space from the model space, in terms of the meshing, opens a whole range of possibilities. As demonstrated, a simulation mesh can be optimized for a given source excitation frequency. Here, our main objective is to present a feasibility study. We have not further explored to which degree one may reduce the spatial simulation mesh sampling without significant loss of accuracy. The demonstration shows a speed-up factor of ≈ 1.8. However, we believe that there exists further potential.

Another benefit from the method arises in the case of very large modeling/inversion domains, where the simulation grid assigned to a particular transmitter might only cover a small subset of the parameter space. In this case, the method offers the capability of a "sliding" simulation mesh. Depending on the location of a source in the model and its resolution coverage of the inversion domain, the simulation mesh can be constantly adapted both in size and position for each different source.

*www.nersc.gov

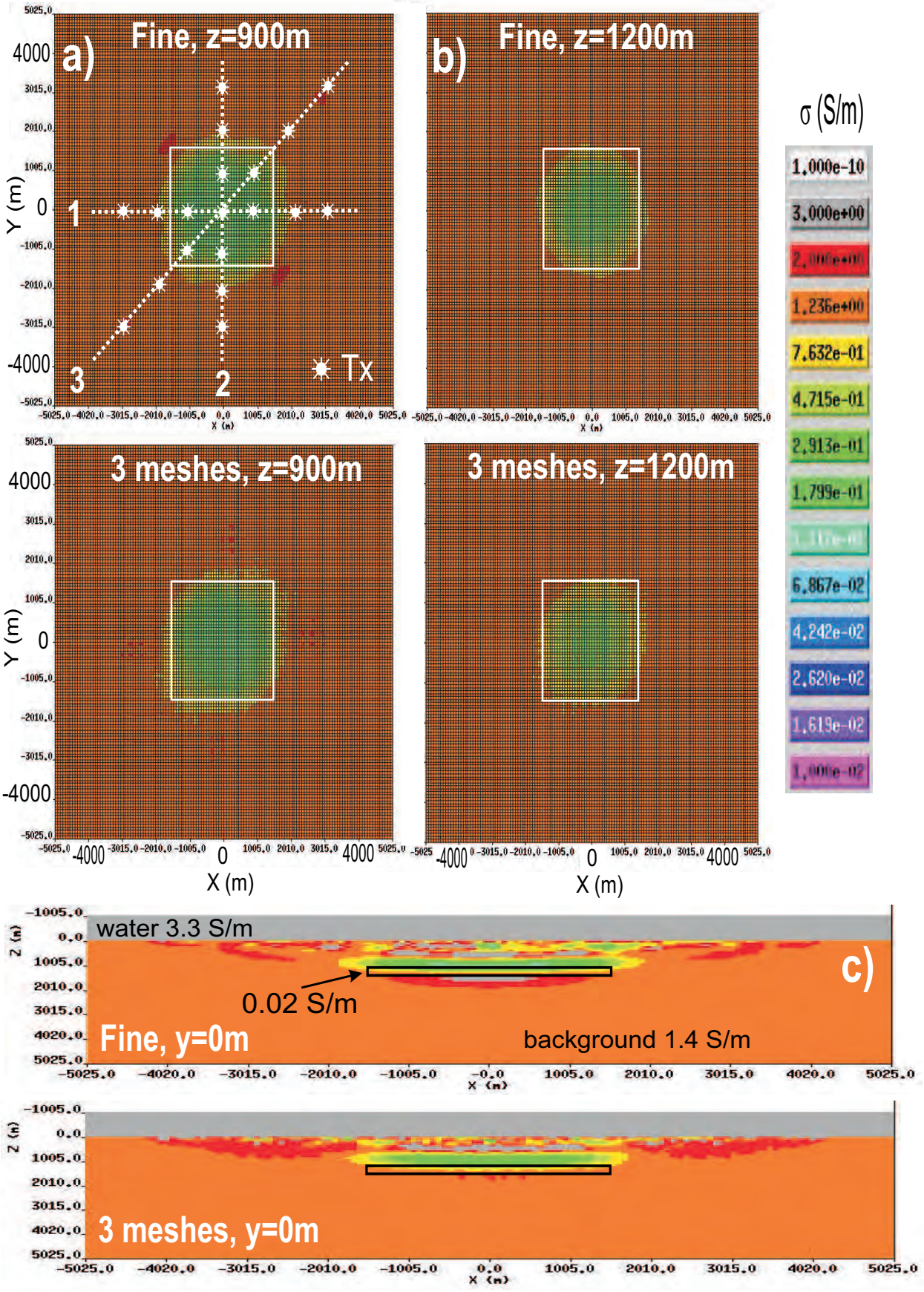

Figure 1: Inversion results after 200 iterations. Upper/lower figures belong to the single/3-mesh results. (a) x-y plot at z=900m, (b) x-y plot at z=1200m, (c) x-z plot at y=0m. The upper left plot also shows a projection of the three profiles. The true model contours are outlined by rectangles.

REFERENCES

Alumbaugh, D. L., Newman, G. A., Prevost, L., and Shadid, J. N., 1996, Three–dimensional wideband electromagnetic modeling on massively parallel computers: Radio Science, 31, 1–23.

Moskow, S., Druskin, V., Habashy, T., Lee, P., and Davydychewa, S., 1999, A finite difference scheme for elliptic equations with rough coefficients using a cartesian grid nonconforming to interfaces: SIAM J. Numerical Analysis, 36, 442–464.

Newman, G. A., and Alumbaugh, D. L., 1997, Three–dimensional massively parallel electromagnetic inversion – I. Theory: Geophys. J. Int., 128, 345–354.

Newman, G. A., and Hoversten, G. M., 2000, Solution strategies for two- and three-dimensional electromagnetic inverse problems: Inverse Problems, 16, 1357-1375.

Yee, K. S., 1966, Numerical solution of initial boundary problems involving Maxwell's equations in isotropic media: IEEE Trans. Ant. Prop., 14, 302–309.

ACKNOWLEDGMENTS

We wish to thank the German Alexander-von-Humboldt (AvH) foundation for support of this work through a Feodor-Lynen-Research Fellowship granted to Michael Commer. This work was carried out at Lawrence Berkeley National Laboratory, with base funding provided by United States Department of Energy, Office of Basic Energy Sciences, under contract DE-AC02-05CH11231, and the Exxon Mobil corporation under Work For Others Agreement.

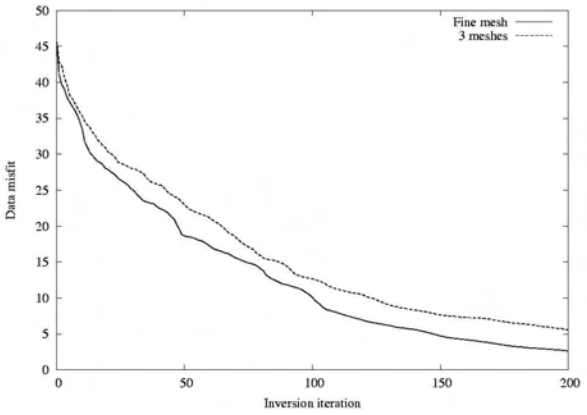

Figure 2: Comparison of the data misfits between the single-mesh and three-mesh inversions.

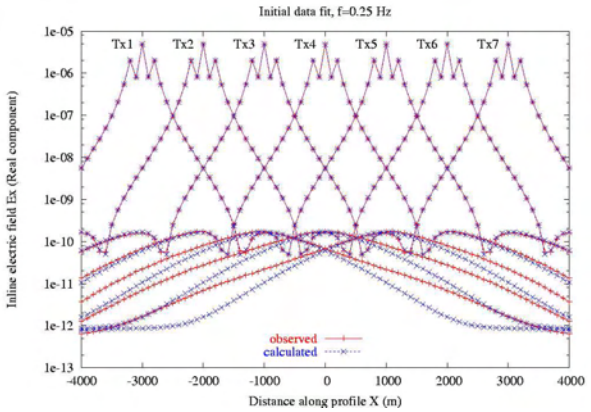

(a)

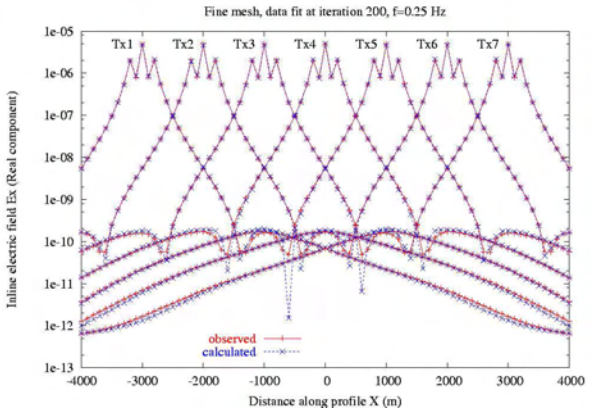

(b)

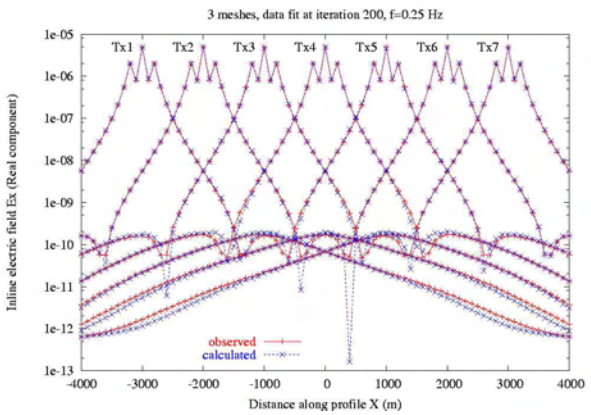

(c)

Figure 3: Data fits for the profile parallel to the x-axis. Initial fit (a), and final fits for the fine-mesh (b) and three-mesh (c) inversions.

EDITED REFERENCES

Note: This reference list is a copy-edited version of the reference list submitted by the author. Reference lists for the 2006 SEG Technical Program Expanded Abstracts have been copy edited so that references provided with the online metadata for each paper will achieve a high degree of linking to cited sources that appear on the Web.

REFERENCES

Alumbaugh, D. L., G. A. Newman, L. Prevost, and J. N. Shadid, 1996, Three–dimensional wideband electromagnetic modeling on massively parallel computers: Radio Science, **31**, 1–23.

Moskow, S., V. Druskin, T. Habashy, P. Lee, and S. Davydychewa, 1999, A finite difference scheme for elliptic equations with rough coefficients using a cartesian grid nonconforming to interfaces: SIAM Journal Numerical Analysis, **36**, 442–464.

Newman, G. A., and D. L. Alumbaugh, 1997, Three–dimensional massively parallel electromagnetic inversion – I. Theory: Geophysical Journal International, **128**, 345–354.

Newman, G. A., and G. M. Hoversten, 2000, Solution strategies for two- and three-dimensional electromagnetic inverse problems: Inverse Problems, **16**, 1357–1375.

Yee, K. S., 1966, Numerical solution of initial boundary problems involving Maxwell's equations in isotropic media: IEEE, Antennas and Propagation, **14**, 302–309.